Direct Localization for Massive MIMO

(article starts on next page)

Direct Localization for Massive MIMO

Nil Garcia *Member, IEEE*, Henk Wymeersch, *Member, IEEE*, Erik G. Larsson, *Fellow, IEEE*
Alexander M. Haimovich, *Fellow, IEEE*, and Martial Coulon

Abstract—Large-scale MIMO systems are well known for their advantages in communications, but they also have the potential for providing very accurate localization thanks to their high angular resolution. A difficult problem arising indoors and outdoors is localizing users over multipath channels. Localization based on angle of arrival (AOA) generally involves a two-step procedure, where signals are first processed to obtain a user's AOA at different base stations, followed by triangulation to determine the user's position. In the presence of multipath, the performance of these methods is greatly degraded due to the inability to correctly detect and/or estimate the AOA of the line-of-sight (LOS) paths. To counter the limitations of this two-step procedure which is inherently sub-optimal, we propose a direct localization approach in which the position of a user is localized by jointly processing the observations obtained at distributed massive MIMO base stations. Our approach is based on a novel compressed sensing framework that exploits channel properties to distinguish LOS from non-LOS signal paths, and leads to improved performance results compared to previous existing methods.

Index Terms—MIMO, multipath channels, position measurement, 5G mobile communication, direction-of-arrival estimation, navigation, antenna arrays, signal processing algorithms, compressed sensing, sparse matrices, parameter estimation, base stations.
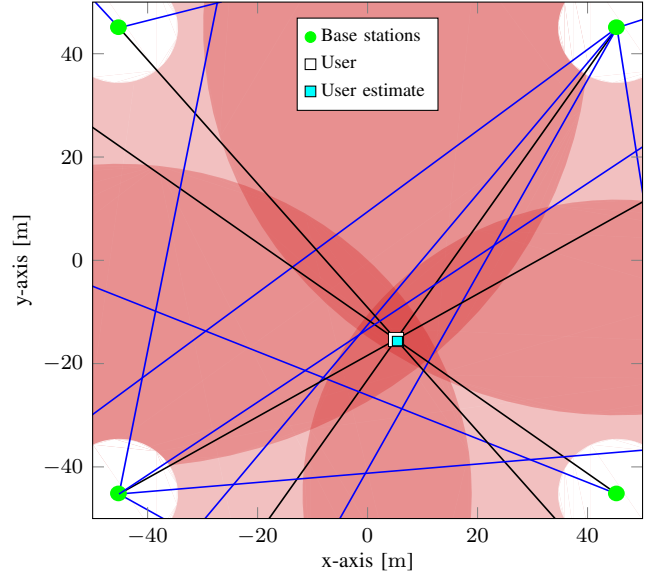
Fig. 1. Example scenario with four base stations. The white circle around each base station excludes the near field region. Each TOA leads to a red disc, the intersection of which is the feasible area. The blue and black lines represent the true bearing lines of the NLOS and LOS paths, respectively.

I. INTRODUCTION

MASSIVE MIMO, a leading 5G technology [1], relies on the use of a large number of antennas at the base station. It has many advantages in cellular communications, including increased spectral efficiency, high directivity, and low complexity [2], [3]. While research on massive MIMO has focused mainly on communications, it is also an enabler for high-accuracy localization [4]. For instance, a finger-printing localization solution is proposed in [5] for locating multiple users by means of distributed massive MIMO. A personal mobile radar with millimeter-wave massive arrays is proposed in [6] and used for simultaneous localization and mapping (SLAM) in [7].

MIMO localization has received significant treatment in the technical literature, generally harnessing angle-of-arrival (AOA) estimation. Typically, a source emits a signal, and then in a *two-step localization* approach, the AOAs are measured at all base stations, and then, the source's location is found

by triangulation. In benign open-air applications, where such methods are referred to as bearings-only target localization (BOTL) good performance can be observed [8]–[10]. However, in dense multipath environments, such as urban areas or inside buildings, the AOA estimates are biased in general. For that reason, pure AOA-based techniques [11] have not been very popular in harsh multipath environments, due to large localization errors [5]. Massive arrays offer the possibility of precisely estimating the AOAs of the individual multipath components thanks to their high angular resolution [12], [13]. Nonetheless, measuring multiple AOAs at each base station requires identification of the AOA of the line-of-sight (LOS) paths. A possible strategy is to select the strongest arrival as LOS [14]. However, the LOS path may be damped or obstructed as it is often the case indoors [15], [16]. Another option is to combine all estimated AOAs in a fusion center and perform data association [17], but this is an NP-hard problem for which the optimal solution cannot be computed efficiently.

An alternative way to tackle localization problems, is to use a *direct localization* approach [18]. Contrary to traditional techniques, the location of the source is estimated directly from the data, without estimating intermediate parameters, such as the AOAs of the LOS paths. The concept of direct localization was first introduced in [19], [20], and later applied to AOA-based localization [21] and, more recently, to hybrid AOA–TOA (time-of-arrival) localization [18], [22]. However,

all these methods were designed for pure LOS environments. Some direct localization techniques [23], [24] targeted to multipath scenarios exist in the literature, but they are not tailored to AOA information and massive arrays. A requirement of direct localization is that the signals, or a function of them, are sent to a fusion center that estimates the source's locations. In general, it is easier to achieve such a topology indoors as the distances are smaller. In the case of cellular networks, cloud radio access networks (C-RAN) [25], [26] may provide the required infrastructure. C-RAN is a novel architecture for wireless cellular systems whereby the base stations relay the received signals to a central unit which performs all the baseband processing.

Our main contribution is a novel localization technique, called Direct Source Localization (DiSouL), that jointly processes the snapshots of data acquired at each base station in order to directly estimate the location of the source. Thanks to the high angular resolution of the massive arrays, the AOAs of the LOS paths can be used to precisely estimate the location of the source. DiSouL relies on a new compressive sensing framework[1] which exploits the fact that LOS components must originate from a common location whereas NLOS components have arbitrary AOAs. Contrary to previous AOA-based existing methods which assume that the LOS path is the strongest, this property enables DiSouL to infer the source position from the LOS AOAs even when the LOS paths are weaker than the NLOS paths. In comparison to ranging-based methods, DiSouL does not require large signal bandwidths in order to position a source accurately. To improve the signal-to-noise-ratio, DiSouL preprocesses the received signals with a matched filter, and then, samples at one time instant. We show how to determine such sampling instant at each base station based on a variation of the threshold matched filter [28]. In addition, two mechanisms are presented to lower the computational burden and increase the accuracy. The first variation uses coarse TOA estimates at each base station to narrow the search area, while the second mechanism relies on a modified version of the grid refinement procedure [29]. Finally, to validate the theory, numerical results are provided, showing that DiSouL can achieve sub-meter accuracy with high probability which is sufficient for many applications (e.g., positioning of users in cellular networks, personal navigation, etcetera). In summary the contributions are:

- A novel localization technique for massive MIMO stations based on AOA information and assisted with TOA estimates.
- The mathematical formulation of a framework that enables the detection and estimation of LOS and NLOS paths without formulating a data-association problem.
- A simple generalization of the threshold matched filter for TOA estimation for arrays of antennas.
- A grid refinement procedure for lowering the computational complexity of the proposed localization technique.

Notation: $\|\cdot\|_1$, $\|\cdot\|_2$ and $\|\cdot\|_{2,1}$ denote the ℓ_1-norm, ℓ_2-norm and $\ell_{2,1}$-norm, respectively, and $\|\cdot\|_0$ is the pseudo-ℓ_0-norm

which counts the number of non-zero elements.

II. SYSTEM MODEL

We consider a two-dimensional scenario with one user (or source) and L massive MIMO base stations equipped with arrays of S_l antennas each. The user is located at $\mathbf{p} = [p^x, p^y]^{\mathrm{T}}$ in an area $\mathcal{R}$ known a priori, the center of gravity of the stations' arrays are located at $\tilde{\mathbf{p}}_l = [\tilde{p}_l^x, \tilde{p}_l^y]^{\mathrm{T}}$ and assumed to be in the far field with respect to the source. All arrays are equipped with fully digital processing, i.e., one radio frequency baseband chain per antenna [30], [31]. We denote by $\mathbf{a}_l(\theta)$ the array response vector at base station l for a ray impinging with angle θ. The array response implicitly accounts for the array configuration and the antenna pattern of each antenna element.

The source broadcasts a known signal $s(t)$ with half-power bandwidth B, which propagates through the multipath environment, resulting in a received signal at base station l given by

$$\mathbf{z}_l(t) = \mathbf{z}_l^{\mathrm{LOS}}(t) + \mathbf{z}_l^{\mathrm{NLOS}}(t) + \mathbf{n}_l(t) \qquad 0 \le t < T_{\mathrm{obs}}, \quad (1)$$

where

$$\mathbf{z}_l^{\mathrm{LOS}}(t) = \alpha_l \, \mathbf{a}_l(\theta_l(\mathbf{p})) \, s(t - \tau_l(\mathbf{p})) \qquad (2)$$

$$\mathbf{z}_l^{\mathrm{NLOS}}(t) = \sum_{m=1}^{P_l} \alpha_l^m \, \mathbf{a}_l(\theta_l^m) s(t - \tau_l^m), \qquad (3)$$

in which T_{obs} is the observation time, each component of $\mathbf{n}_l(t)$ is white Gaussian noise with spectral density N_0, α_l is an unknown complex scalar, θ_l and τ_l are the angle of arrival (AOA) and time of arrival (TOA), all related to the line of sight (LOS) path, while α_l^m, θ_l^m, and τ_l^m are the channel gain, AOA, and TOA of the m-th NLOS component, for the P_l NLOS path. All these parameters are unknown. The signal is narrowband with respect to the arrays, i.e., at each array l the amplitudes $\{\alpha_l\}$, $\{\alpha_l^m\}$ do not change across antennas. The LOS parameters $\tau_l(\mathbf{p})$ and $\theta_l(\mathbf{p})$ are related to the source position through

$$\tau_l(\mathbf{p}) = \|\mathbf{p} - \tilde{\mathbf{p}}_l\|/c \qquad (4)$$

$$\theta_l(\mathbf{p}) = \arctan\left(\frac{p^y - \tilde{p}_l^y}{p^x - \tilde{p}_l^x}\right) + \pi \cdot \mathbb{1}\left(p^x < \tilde{p}_l^x\right), \quad (5)$$

where c is the speed of light, while the range of the arctangent function is $-\pi/2 \le \arctan(x) < +\pi/2$, the angle is computed with respect to the x-axis and anticlockwise, and $\mathbb{1}(\mathsf{P})$ is one if the logical expression P is true[2]. Let $\tilde{\mathbf{p}}_{l,a} = [\tilde{p}_{l,a}^x, \tilde{p}_{l,a}^y]^T$ be the position of antenna a at BS l, relative to the array's center of gravity. For arrays without mutual antenna coupling and isotropic antennas, the array response $\mathbf{a}_l(\theta)$ for a given AOA θ admits the following close-form expression

$$[\mathbf{a}_l(\theta)]_a = \exp\left(\frac{2\pi i}{\lambda} \tilde{\mathbf{p}}_{l,a}^{\mathrm{T}} \begin{bmatrix} \cos(\theta) \\ \sin(\theta) \end{bmatrix}\right), \qquad (6)$$

where $[\cdot]_a$ denotes the a-th component, i is the imaginary unit and λ is the wavelength of the carrier. In practice, for non-ideal

---

[1]Briefly introduced in the conference paper [27] but without mathematical justification and for the case of TOA-based localization instead.

[2]The summand $\pi \cdot \mathbb{1}\left(p^x < \tilde{p}_l^x\right)$ is added for resolving the ambiguity caused by the fact that $\arctan(y/x) = \arctan(-y/-x)$.

threshold:

$$\hat{\tau}_l = \text{find-1st-peak} \left\{ z_l^{\text{NC}}(t) : z_l^{\text{NC}}(t) \geq \eta \right\}. \qquad (10)$$

In practice, values of $z_l^{\text{NC}}(t)$ may only be available at discrete instants. In such case the location of the peak may be obtained by parabolic fitting [32]. Following [28], the threshold is selected so that the probability of early false alarm is very low. An early false alarm event is defined as detecting a peak due to noise before the true TOA of the LOS path. Since the threshold MF ignores second and later peaks (above the threshold), the following expression on the probability of false alarms only considers those peaks happening before the LOS TOA. When the false alarm probability is small, it can be approximated as [28]

$$P_{\text{FA}} \approx 1 + \frac{(1 - q_{\text{noise}})^{N_{\text{TOA}}} - 1}{N_{\text{TOA}} \, q_{\text{noise}}}, \qquad (11)$$

where $N_{\text{TOA}} = T_{\text{obs}}/T_{\text{corr}}$ and T_{corr} is the waveform correlation time, which for most types of waveforms, is well approximated by the inverse of the bandwidth $T_{\text{corr}} = 1/B$. The term q_{noise} is defined as the probability that the noise in absence of signal exceeds threshold η

$$
\begin{aligned}
q_{\text{noise}} &= \text{Prob} \left(\left\| \mathbf{n}_l^{\text{MF}}(t) \right\|_2^2 \geq \eta \right) \\
&= 1 - F_{2S_l} \left(\frac{2\eta}{\sigma^2} \right),
\end{aligned} \qquad (12)
$$

where S_l is the number of antennas at BS l, σ^2 is the noise variance at each antenna, and $F_k(x)$ be the cumulative distribution function of the Chi-squared distribution with k degrees of freedom evaluated at x. The threshold η resulting in the desired P_{FA} can be found by performing a one-dimensional search of (11).

Assuming all TOA estimates are positively biased, then we can create a set

$$\mathcal{F} = \left\{ \boldsymbol{\pi} \in \mathbb{R}^2 : \| \boldsymbol{\pi} - \mathbf{p}_l \|_2 \leq c \, \hat{\tau}_l, \forall l \right\} \qquad (13)$$

and narrow the search area to $\mathcal{R} \cap \mathcal{F}$ instead of $\mathcal{R}$. In the unlikely event that not all TOA estimates are positively biased, it is possible that $\mathcal{F} = \emptyset$. In such a case, we expand $\mathcal{F}$ by increasing all TOA estimates by a constant value v until $\mathcal{F} \neq \emptyset$. We have chosen $v = 1/B$, where B is the signal bandwidth, though the value of v turns out to not be critical for the localization performance. Reducing the search area has two benefits. On one hand it lowers the computational complexity of the optimization problem that is proposed in the next section. On the other hand it can positively affect the accuracy of the localization procedure.

C. Sampling Times

The outputs of the matched filters (8) at all base stations (8) are sampled at times $\{t_l\}_{l=1}^L$. Contrary to the estimation of the TOAs $\{\hat{\tau}_l\}_{l=1}^L$, the goal is to sample $\{\mathbf{z}_l^{\text{MF}}(t)\}_{l=1}^L$ at an instant where there is as little as possible NLOS interference and as much as possible energy from the LOS component. One solution would be to sample at the same time than the TOA estimates, however, due to their bias, we will rarely

sample at the time of maximum LOS energy, and moreover, the NLOS interference may be very large as well. We propose an alternative strategy, which has been verified numerically to lead to better results in Section VI for the propagation conditions under consideration. The idea is to use the same threshold matched filter for TOA estimation, but instead of selecting the time of the first peak, we select the instant when the received signal crosses the threshold for the first time, i.e.,

$$t_l = \min \left\{ t : z_l^{\text{NC}}(t) \geq \eta \right\}. \qquad (14)$$

Comparing the expression of the sampling time to that of the TOA estimate (10), it follows that $t_l \leq \hat{\tau}_l$ for all l.

D. Localization

To solve the localization problem, we rely on tools from compressive sensing. Specifically, we propose a grid-based approximate solution to the problem of localizing a source on a continuous map which exploits the notion of sparsity and row-sparsity [33]. To this end, first we introduce a uniform grid of Q locations

$$\mathcal{L} = \{ \boldsymbol{\pi}_1, \ldots, \boldsymbol{\pi}_Q \} \subset \mathcal{R} \cap \mathcal{F}, \qquad (15)$$

and a uniform grid of M_l angles for each base station array

$$\mathcal{A}_l = \{ \vartheta_1, \ldots, \vartheta_{M_l} \} \subset [0, 2\pi). \qquad (16)$$

The main assumption here is that the source is positioned on a grid location, and that the AOAs of the NLOS paths are also in the grid of angles. While beamforming suffers from the Rayleigh resolution limit [34], which is independent of the SNR, an advantage of sparsity-based techniques is that they can resolve multipath components within a Rayleigh cell (i.e., achieve super-resolution) [29], [35], [36].

Let $\mathbf{X} \in \mathbb{C}^{Q \times L}$ be a matrix whose entry on row q, column l is denoted by x_{ql} and represents the complex gain of a LOS path from grid location $\boldsymbol{\pi}_q$ to base station l. Let y_{ml} be the complex gain of a NLOS path arriving at the l-th base station with angle ϑ_m. Then, by definition, only one row in $\mathbf{X}$ is different from zero, and $y_{ml} \neq 0$ only if ϑ_m is equal to the AOA of a NLOS path at base station l. Thus, if the grids are dense enough, $\mathbf{X}$ is row-sparse and $\mathbf{y}_l$ is sparse for all l. It is well known in the compressive sensing literature [37], that row sparsity can be induced by minimizing the $\ell_{2,1}$-norm, i.e. $\| \mathbf{X} \|_{2,1} = \sum_{q=1}^Q \sqrt{\sum_{l=1}^L |x_{ql}|^2}$, and that sparsity can be induced by minimizing the ℓ_1-norm, i.e. $\| \mathbf{y}_l \|_1 = \sum_{m=1}^{M_l} |y_{ml}|$ where $\mathbf{y}_l = [y_{1l}, \ldots, y_{M_l l}]^{\text{T}}$. Thus, with all this in mind, we propose to solve the following optimization problem

$$\min_{\mathbf{X}, \mathbf{y}_l} \quad w \| \mathbf{X} \|_{2,1} + \sum_{l=1}^L \| \mathbf{y}_l \|_1 \qquad (17a)$$

$$\text{s.t.} \quad \sum_{l=1}^L \| \bar{\mathbf{z}}_l - \hat{\mathbf{z}}_l \|_2^2 \leq \epsilon \qquad (17b)$$

$$\hat{\mathbf{z}}_l = \sum_{q=1}^Q x_{ql} \mathbf{a}_l \left(\theta_l(\boldsymbol{\pi}_q) \right) + \sum_{m=1}^M y_{ml} \mathbf{a}_l \left(\vartheta_m \right), \forall l. \quad (17c)$$

This is a second-order cone program (SOCP) for which very efficient solvers exist. The optimization variables are $\mathbf{X}$ and $\{\mathbf{y}_l\}_{l=1}^L$. The vector $\hat{\mathbf{z}}_l$ as defined in (17c) is a reconstruction of $\bar{\mathbf{z}}_l$ for a given choice of $\mathbf{X}$ and $\{\mathbf{y}_l\}_{l=1}^L$. The parameter ϵ establishes the maximum allowed mismatch between the observations and the reconstruction.

Intuitively, problem (17) seeks the sparsest number of source locations and NLOS paths that can describe the observations $\{\bar{\mathbf{z}}_l\}$. Precisely, minimizing $\|\mathbf{X}\|_{2,1}$, induces a sparse number of source locations (hopefully a single location), and minimizing $\sum_{l=1}^L \|\mathbf{y}_l\|_1$, induces a sparse number of NLOS paths. These are two different types of sparsity, and therefore, in order to combine them together some kind of balancing coefficient or weight w needs to be added. Intuitively, the parameter w ensures that not all signal energy is assigned to only LOS or NLOS components. In particular, if $w = 0$, the objective function is not penalized by filling matrix $\mathbf{X}$ with non-zeros, thus, the reconstruction will always favor a representation based on LOS paths rather than NLOS paths. On the contrary, if $w \to \infty$, then the objective function will highly penalize any non-zero in matrix $\mathbf{X}$, thus, the reconstruction will always favor a representation based on NLOS paths. Thus, it is clear than in our multipath scenario, consisting of LOS and NLOS paths, if a suitable w exists, it must be larger than 0 and finite. Below suitable choices for ϵ and w are proposed.

Remark: While this technique searches a source on a plane, it can be generalized to a three-dimensional search, at a cost of computational complexity. It is also possible that the technique may improve its robustness against multipath because in two dimensions two distinct NLOS bearing lines always intersect but in three dimensions they generally do not.

IV. PARAMETER SELECTION

In this section, we motivate the choice for ϵ and w in the optimization problem of Section III-D. The choices do not guarantee recovery of the correct position and are derived under simplified assumptions.

A. Setting the Parameter ϵ

The parameter ϵ in (17) defines the allowed mismatch between the observations and the reconstruction. Typically, ϵ is a bound on the noise. Since the noise is Gaussian, it is unbounded, and instead ϵ is chosen so that it is a bound with high probability, i.e.

$$\text{Prob}\left(\sum_{l=1}^L \|\bar{\mathbf{n}}_l\|_2 \le \epsilon\right) = \gamma. \tag{18}$$

where γ is, for example, 0.99. Because $\bar{\mathbf{n}}_l$ are random white Gaussian vectors of length S_l, it follows that the error normalized by the noise variance $2\sigma^{-2}\sum_{l=1}^L \|\bar{\mathbf{n}}_l\|_2$ is a Chi-squared random variable with $2\sum_{l=1}^L S_l$ degrees of freedom. Let $F_k(x)$ be the cumulative distribution function of the Chi-squared distribution with k degrees of freedom evaluated at x and $F_k^{-1}(y)$ its inverse function evaluated at y. Then, the value of ϵ can be computed as

$$\epsilon = \frac{\sigma^2}{2} F_{2\sum_{l=1}^L S_l}^{-1}(\gamma). \tag{19}$$

In low SNR conditions, it is possible that the aggregated energy of all snapshots is not larger than ϵ, i.e.

$$\sum_{l=1}^L \|\bar{\mathbf{z}}_l\|_2^2 \le \epsilon, \tag{20}$$

making problem (17) have the trivial all-zeros solution, thus, failing to estimate the location of the source. In this case we propose to simply look up the location whose LOS components correlate the most with the snapshots:

$$\hat{\mathbf{p}} = \arg\max_{\boldsymbol{\pi} \in \mathcal{L}} \sum_{l=1}^L \frac{\left|\mathbf{a}_l^{\mathrm{H}}(\theta_l(\boldsymbol{\pi}))\bar{\mathbf{z}}_l\right|^2}{\|\mathbf{a}_l(\theta_l(\boldsymbol{\pi}))\|_2^2}. \tag{21}$$

B. Setting the Parameter w

In order to obtain an expression for w, we will not prove that the AOAs are correctly recovered by solving (17), but rather that, under proper selection of w, if the AOAs are correctly recovered, then they can also be correctly identified as either LOS or NLOS. The key property that will dictate the value of w, and in turn estimate the correct source location is based on the following definition.

Definition 1 (consistent location)**.** *A location $\boldsymbol{\pi}$ is consistent with L paths, if the AOAs of the direct paths between $\boldsymbol{\pi}$ and the base stations are true AOAs, i.e.*

$$\theta_l(\boldsymbol{\pi}) \in \Theta_l \quad \text{for } l = 1, \ldots, L, \tag{22}$$

where Θ_l is the set of true AOAs at base station l

$$\Theta_l = \left\{\theta_l(\mathbf{p}), \theta_l^1, \ldots, \theta_l^{P_l}\right\}. \tag{23}$$

By definition, the true source location $\mathbf{p}$ is consistent with the L paths because the LOS components travel in a straight line. To find a criterion for the weight, we restrict ourselves to a simplified version of the problem and then later evaluate the criterion in a more realistic setting. Our analysis on the weight criterion is limited through the three following assumptions.

A1) Besides the source location $\mathbf{p}$, no other location is consistent with L paths.

A2) The grids $\mathcal{L}$ and $\{\mathcal{A}_l\}_{l=1}^L$ are sufficiently dense to contain the source location $\mathbf{p}$ and all AOAs, respectively.

A3) Denoting by $\hat{\Theta}_l$ the estimated AOAs at base station l, i.e.

$$\hat{\Theta}_l = \{\theta_l(\boldsymbol{\pi}_q) : x_{ql} \ne 0\} \cup \{\vartheta_{ml} : y_{ml} \ne 0\}, \tag{24}$$

then $\hat{\Theta}_l = \Theta_l, \forall l$. In other words, the solution of (17) is able to recover the true AOAs. This assumption is reasonable in high SNR conditions.

These assumptions are only used for deriving a suitable value of w. In practice, in realistic multipath environments, some of these assumptions may break down. Thus, in Section VI, the proposed method is tested versus a realistic indoor multipath channel model, and shown to recover the user position with sub-meter accuracy and high probability.

Lemma 1. *Assume A2) and A3). If $w > \sqrt{L-1}$, then any estimated location output by problem (17) is consistent with L paths (in the sense of Definition 1).*

Proof. See Appendix A. □

Lemma 2. *Assume A2) and A3). If $w < \sqrt{L}$, then problem (17) outputs at least one location (i.e. $\mathbf{X} \neq \mathbf{0}$).*

Proof. See Appendix B. □

The two lemmas lead directly to the following theorem, which guarantees the correct recovery of the source location.

Theorem 1. *If Assumptions A1), A2), and A3) hold, then a sufficient condition for the correct recovery of the source location is*

$$\sqrt{L-1} < w < \sqrt{L}. \tag{25}$$

Proof. If $w < \sqrt{L}$, by Lemma 2 al least one estimated location is output by problem (17). Moreover, if $w > \sqrt{L-1}$, by Lemma 1 any estimated location is consistent with L paths. However, according to Assumption A1), only the location of the source is consistent with L paths, thus completing the proof. □

C. The Case of Non-LOS

In practice, BSs may be in non-line-of-sight (NLOS) because the LOS paths are blocked or attenuated (making the LOS path pass undetected). The proposed technique relies on the presence of the L LOS paths for achieving high precision localization, and it may break down when the base stations are in NLOS. If the weight in (17a) is chosen according to Lemma 1, any location estimate output by problem (17) must be consistent with L paths. However, if one base station is in NLOS, then the source will only be consistent with $L-1$ paths, and therefore, the location of the source will not be a solution to (17). Thus, adjusting the weight requires a priori knowledge of the number of LOS base stations. We can adjust the weight as follows. Let L^* be the number of base stations in LOS with the source, and let $\hat{L}$ be an estimate of L^*. Obviously, $L^* \leq L$. Furthermore, assume no other location besides the location of the source is consistent with L^* paths. We start by assuming that all base stations are in LOS, i.e. $\hat{L} = L$, set the weight according to Theorem 1, and solve problem (17). According to Lemma 1, the location of the source will be estimated only if it is consistent with $\hat{L}$ paths. If $L^* < \hat{L}$, the solver will return $\mathbf{X} = \mathbf{0}$. When this event is detected, $\hat{L}$ can be reduced and (17) solved again. This procedure can be repeated as shown in Algorithm 1. Note that if $\mathbf{X} \neq \mathbf{0}$, the location with strongest gains is returned as the estimate $\hat{\mathbf{p}}$ (see lines 10–11). Theoretically speaking, since two non-parallel paths always intersect on the plane, to ensure that we can distinguish LOS from NLOS paths, and in turn, recover the user position, the number of LOS BSs should be $L^* \geq 3$. However, when the LOS paths are the strongest, we have verified numerically, that the user can be recovered with $L^* = 2$ as well.

Based on the choices for ϵ and w, Algorithm 1 summarizes the proposed solution strategy.

V. GRID REFINEMENT

Dense grids of locations and angles are necessary to achieve fine resolution, but making the grids too dense results in large

---

Algorithm 1 Direct Localization

1: set $\hat{L} = L$ and $\hat{\mathbf{p}} = \emptyset$
2: set ϵ according to (19)
3: **if** $\sum_{l=1}^{L} \|\bar{\mathbf{z}}_l\|_2^2 > \epsilon$ **then**
4:     **while** $\hat{\mathbf{p}} = \emptyset$ and $\hat{L} > 1$ **do**
5:         set $w = \sqrt{\hat{L}} - 0.5$
6:         solve (17) to obtain $\mathbf{X}$ and $\mathbf{y}_l, \forall l$
7:         **if** $(\mathbf{X} \equiv \mathbf{0})$ **then**
8:             $\hat{L} \leftarrow \hat{L} - 1$
9:         **else**
10:            $\hat{q} = \arg\max_q \|\mathbf{X}_{q,:}\|_2$
11:            $\hat{\mathbf{p}} = \boldsymbol{\pi}_{\hat{q}}$
12:         **end if**
13:     **end while**
14: **else**
15:     estimate $\hat{\mathbf{p}}$ by (21)
16: **end if**

---

computation time. The computational complexity of solving (17) scales as $\mathcal{O}((QL + \sum_l M_l)^{3.5})$ [38], where Q and M are the number grid locations and angles respectively, and L is the number of base stations. This motivates an adaptive grid-refinement strategy originally proposed in [29]. The idea behind the grid refinement approach is to start with a coarse grid of locations and angles; subsequently, the grid is refined around the estimated locations and angles and the optimization problem (17) is solved again. This procedure can be repeated until a certain grid resolution has been achieved or a stopping criterion has been met. Thus, the benefits of grid refinement are two-fold: lower computational complexity and fine grid resolution.

In comparison to previous grid refinement approaches [29], [39], ours is more complex due to the two different types of grids used to describe the observed data. At iteration k of the grid refinement process, we will denote the position grid by $\mathcal{L}^{(k)}$ and the angle grid (for base station l) by $\mathcal{A}_l^{(k)}$. At iteration $k = 0$, the grids are uniform over $\mathcal{R} \cap \mathcal{F}$ and $[0, 2\pi)$, respectively. The resolutions in $\mathcal{L}^{(0)}$ and $\mathcal{A}_l^{(0)}$ are set to $\pi_{\text{res}} \in \mathbb{R}_+$ and $\vartheta_{\text{res}} \in \mathbb{R}_+$, respectively. Define the following operators:

$$\text{grid}(\hat{\Pi}, \delta) = \{\boldsymbol{\pi} \in \mathbb{R}^2 : \boldsymbol{\pi} = \hat{\boldsymbol{\pi}} + [i \; j]^{\text{T}}\delta, \tag{26}$$
$$\hat{\boldsymbol{\pi}} \in \hat{\Pi}, i, j \in \{-2, -1, 0, 1, 2\}\}$$
$$\text{grid}(\hat{\Theta}_l, \delta) = \{\theta \in [0, 2\pi) : \theta = \hat{\theta} + i\delta, \tag{27}$$
$$\hat{\theta} \in \hat{\Theta}_l, i \in \{-2, -1, 0, 1, 2\}\}.$$

We can then set $\mathcal{L}^{(k)} = \text{grid}(\hat{\Pi}, \pi_{\text{res}}/2^k)$ and $\mathcal{A}_l^{(k)} = \text{grid}(\hat{\Theta}_l, \vartheta_{\text{res}}/2^k) \cup \{[\theta_l(\boldsymbol{\pi})]_{\vartheta_{\text{res}}/2^k} : \boldsymbol{\pi} \in \hat{\Pi}\}$, where $[x]_y$ rounds x to the nearest multiple of y. Each successive grid of locations and angles includes the estimated points and their neighboring points. In this case we have chosen to include twenty-four and four neighbor points for the position grid and angle grid, respectively, but other choices of neighbors are possible as well. In addition, the grid of angles also incorporates the angles related to the estimated locations. It

has been empirically verified that this is necessary for the correct performance of this grid refinement approach.

Because at each step the previously estimated points are included in the next grid, the solution at step k is a feasible solution at step $k + 1$. This ensures that the optimum value of the optimization problem (17) cannot increase as iterations progress. Since the objective function is bounded from below by zero, by the monotone convergence theorem [40], the grid refinement procedure must converge. In practice, the refinement process is halted when the progress between two consecutive steps is negligible. Denote as $f_{\text{opt}}^{(k)}$ the optimum value of problem (17) at step k, then the grid refinement is stopped at step k if

$$\frac{\left| f_{\text{opt}}^{(k-1)} - f_{\text{opt}}^{(k)} \right|}{f_{\text{opt}}^{(k-1)}} < \beta, \tag{28}$$

where β is a small value, e.g., $\beta = 10^{-3}$.

Algorithm 2 Grid refinement

1: given a coarse grids of locations $\mathcal{L}^{(0)}$ and angles $\mathcal{A}_l^{(0)}, \forall l$
2: set $k = 0$
3: **while** (28) not satisfied **do**
4:     solve (17) with $\mathcal{L} = \mathcal{L}^{(k)}$ and $\mathcal{A}_l = \mathcal{A}_l^{(k)}$
5:     extract locations $\hat{\Pi} = \{ \boldsymbol{\pi}_q^{(k)} \in \mathcal{L}^{(k)} : \|\mathbf{x}_q^{(k)}\|_2 \neq 0 \}$
6:     extract angles $\hat{\Theta}_l = \{ \vartheta_{ml}^{(k)} \in \mathcal{A}_l^{(k)} : y_{ml}^{(k)} \neq 0 \}, \forall l$
7:     increase k
8:     set $\mathcal{L}^{(k)} = \text{grid}(\hat{\Pi}, \pi_{\text{res}}/2^k)$
9:     trim grid of locations $\mathcal{L}^{(k)}$ through TOA assistance
10:     set

$$\mathcal{A}_l^{(k)} = \text{grid}(\hat{\Theta}_l, \vartheta_{\text{res}}/2^k) \cup \{ [\theta_l(\boldsymbol{\pi})]_{\vartheta_{\text{res}}/2^k} : \boldsymbol{\pi} \in \hat{\Pi} \}$$

11: **end while**

A. The DiSouL Algorithm

The summary of the DiSouL algorithm is now presented, comprising the basic Algorithm 1, as well as the TOA assistance of Section III-B and the grid refinement of Section V.

Algorithm 3 DiSouL

1: set η using (11) for the desired P_{FA} (e.g., $P_{\text{FA}} = 10^{-2}$)
2: estimate TOAs $\{\hat{\tau}_l\}_{l=1}^L$ using (10)
3: create initial grid of locations $\mathcal{L}^{(0)}$ and angles $\mathcal{A}_l^{(0)}, \forall l$
4: trim grid of locations through TOA assistance
5: compute sampling times $\{t_l\}_{l=1}^L$ using (14)
6: obtain the snapshots of data by applying MF and sampling at instants $\{t_l\}_{l=1}^L$ as in (8)
7: estimate source location $\hat{\mathbf{p}}$ by Algorithm 1 where line 6 is replaced with Algorithm 2

VI. NUMERICAL RESULTS

In this section, we illustrate the performance of the localization method and compare it to other existing techniques. Unless otherwise stated, all numerical examples are run using the following parameters. The source is positioned randomly
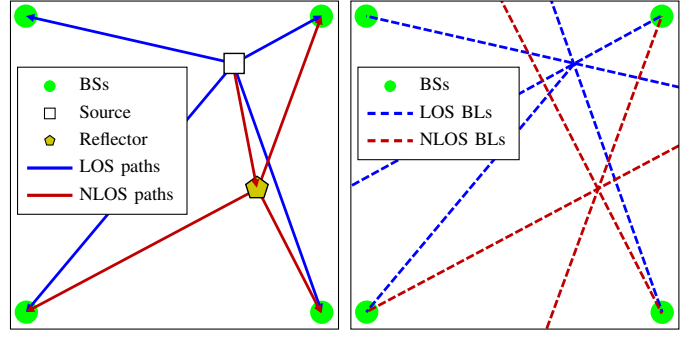
Fig. 2. The left figure plots the LOS and NLOS paths and the right figure plots the bearing lines (BLs). The top left corner base station only receives the LOS path.
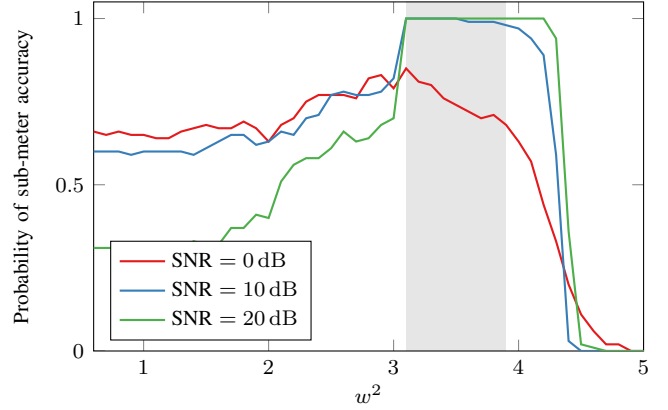
Fig. 3. Probability of sub-meter accuracy versus the choice of the weight for the scenario in Fig. 2. Probability estimated by Monte Carlo simulation where the random parameters are the signal strengths and phases. In grey the area comprising the tested values of w satisfying Theorem 1.

within an area of size $100\,\text{m} \times 100\,\text{m}$. Four base stations are positioned at the corners; if the origin of the coordinate system is taken to be in the middle of the area, the base stations are at coordinates $[45\,\text{m}, 45\,\text{m}]$, $[45\,\text{m}, -45\,\text{m}]$, $[-45\,\text{m}, 45\,\text{m}]$ and $[-45\,\text{m}, -45\,\text{m}]$. The carrier frequency is $7\,\text{GHz}$ and the wavelength $43\,\text{mm}$. Every base station is equipped with a 70-antenna uniform circular array (UCA) [41] with a radius of $24\,\text{cm}$ because it makes the inter antenna spacing equal to half wavelength. We opt for UCAs instead of uniform linear arrays (ULAs) because for the same number of antennas and equal inter antenna spacing, their far field region [42] starts at a much shorter distance ($11\,\text{m}$ for a UCA and $51\,\text{m}$ for a ULA), and contrary to ULAs, UCAs have equal angular resolution towards all directions on the plane. Also, we simulate four base stations because it makes positioning a bit more robust to multipath than using only three base stations[5] while keeping the number of BSs to a reasonable number. The initial grid resolutions of DiSouL are $\pi_{\text{res}} = 5\,\text{m}$ and $\vartheta_{\text{res}} = 5.71°$.

A. *Validation of Theorem 1*

To illustrate Theorem 1, we synthesize a set of snapshots (8) according to the scenario plotted in Fig. 2 and ignore any time delay information. The source is positioned at $[18\,\mathrm{m}, 31\,\mathrm{m}]$ and a reflector is positioned at $[25\,\mathrm{m}, -7\,\mathrm{m}]$. As visualized in Fig. 2, all base stations receive a LOS component, and except for the top left base station, they also receive a NLOS component bounced from the reflector. From Fig. 2, it is apparent that the source location is consistent with 4 paths, the reflector is consistent with 3 paths, and all other locations in that area are consistent with 2 paths or less. We hypothesize that for a sufficiently fine grid, and for a sufficiently high SNR, the probability of recovering the correct source location will be high if the weight is picked according to Theorem 1. The SNR_l for the snapshots (8) is defined as $\mathrm{SNR}_l = S_l\, \mathbb{E}\{|\bar{\alpha}_l|^2\}/\mathbb{E}\{\|\bar{\mathbf{n}}_l\|_2^2\} = \mathbb{E}\{|\bar{\alpha}_l|^2\}/\sigma^2$ and is equal for all base stations $\mathrm{SNR}_l = \mathrm{SNR}$. Every data point in Fig. 3 is generated by running 100 Monte Carlo runs, where at each run the signal strengths and phases of all multipath components are randomized according to Rayleigh and uniform distributions, respectively. The location of the source is estimated by running Algorithm 2, wherein the solution to optimization problem (17) is obtained by the solver Mosek [43]. Fig. 3 plots the empirical probability that the localization error is smaller than $1\,\mathrm{m}$ as a function of w^2. According to Theorem 1, a sufficient condition for recovering the location of the source is that the square of the weight satisfies $L - 1 \le w^2 \le L$. The figure shows that, in this case, for $L = 4$, the range of values $w^2 \in [3, 4]$ yields the correct source location with sub-meter accuracy with probability 1 for a sufficient high SNR.

B. *Localization Performance in Realistic Multipath Channel*

In this section, we perform Monte Carlo simulations in which DiSouL is compared to indirect and direct localization techniques:

1) SR-LS [44], using TOA obtained by the time delay estimator of Section III-B. SR-LS takes as inputs a set of ranges (related to the TOAs by the speed of light) obtained at distributed BSs and outputs the user position by solving a least-squares (LS) fit. Because the maximum likelihood (ML) solution does not lead to a convex optimization problem, the LS solution is only an approximation.
2) IV [10], using AOA information, obtained by applying beamforming [45] on the snapshots (8) and selecting the angle associated with the strongest peak. IV is a closed-form estimator that uses the AOAs measured at distributed BSs to triangulate the user position. In pure LOS environments, IV is consistent and asymptotically (with the number of BSs) unbiased.
3) The Stansfield estimator [8], using hybrid TOA-AOA. The Stansfield estimator is sometimes described as an AOA-based only estimator. It uses coarse range estimates in order to approximate the AOA-based ML

estimator (in absence of multipath) by a closed-form solution. Its formula is a refined version of IV.
4) DPD [18], a direct localization hybrid TOA-AOA technique, operating directly on the received signals (1)–(3). DPD is essentially the ML estimator for a pure LOS environment when directly operating on the received signals. Since the received signals depend on the user position through their AOAs and TOAs, DPD is the optimal hybrid technique in absence of multipath. In practice it requires computing a figure of merit for each grid location on the map, and the one yielding the largest value is the user's position estimate. Due to this two-dimensional search, it is, in general, more computationally expensive than indirect techniques.

The AOAs for IV and the Stansfield estimator are estimated by performing beamforming. More sophisticated AOA estimation techniques, such as MUSIC [46], are not applicable because they require multiple snapshots and break down in the presence of multiple correlated arrivals such as is the case of multipath. A high precision alternative to beamforming is ℓ_1-SVD [29]. However, we have observed in our numerical results that ℓ_1-SVD performs similar to beamforming due to the fact that the AOA estimation errors are caused by peak ambiguities and not the lack of angular resolution. Thus, errors happen mostly when the LOS component is attenuated or blocked by obstacles.

The source emits a Gaussian pulse $s(t)$ at $7\,\mathrm{GHz}$ carrier frequency. We simulate the received signal at each antenna after down-conversion to baseband and sampling. An oversampling factor of 3 is used. It is a assumed a half power bandwidth of $B = 30\,\mathrm{MHz}$ and $10\log_{10}\frac{E}{N_0} = 10\,\mathrm{dB}$, where $E = \mathbb{E}\,|\alpha_l|^2$ is the energy of the received LOS component before sampling (2) (same energy for all l) and N_0 is the noise spectral density at each antenna.

Every data point in the figures is generated by running 1000 Monte Carlo runs. The parameters randomized at each Monte Carlo run are the multipath channels, the noise and the position of the user. The parameters of the multipath channel (1) are generated according to the statistical indoor channel model in [15], the user position is drawn from the uniform distribution over the search area, and the noise is independent and identically Gaussian distributed. In regards to the indoor multipath channel, the parameters' values are those of the Clyde building: cluster decay rate is $34\,\mathrm{ns}$, ray decay rate is $29\,\mathrm{ns}$, cluster arrival rate is $1/17\,\mathrm{ns}$, ray arrival rate is $1/5\,\mathrm{ns}$ and angular variance is $26°$. On the average, at every base station, 99.9% of the energy in the snapshot (8) is contained in 8 discrete multipath arrivals, which, in general, have closely spaced AOAs.

Fig. 4 plots the cumulative density function of the localization error. Clearly, DiSouL achieves high precision accuracy with high probability, followed by DPD and the two-step approaches. To gain a more in-depth understanding, we will focus on the performance of the estimators at sub-meter errors, as a function of E/N_0, bandwidth, number of antennas, channel properties, and calibration errors.

In Fig. 5, the probability of sub-meter precision is shown as a function of E/N_0. Note that DiSouL outperforms all

---

[5]Because on a plane two non-parallel straight lines always intersect, three is the minimum number of BSs needed in order to discriminate LOS from NLOS paths
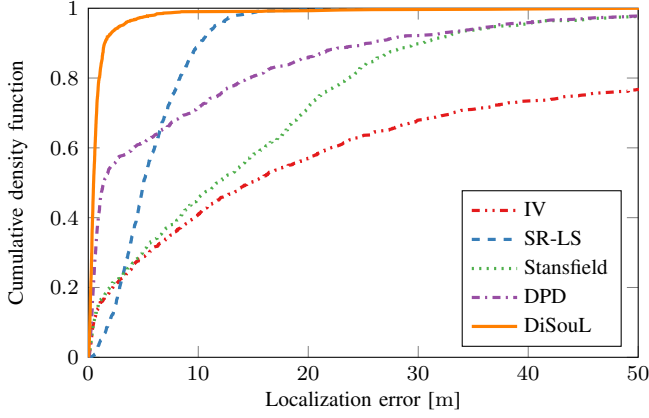
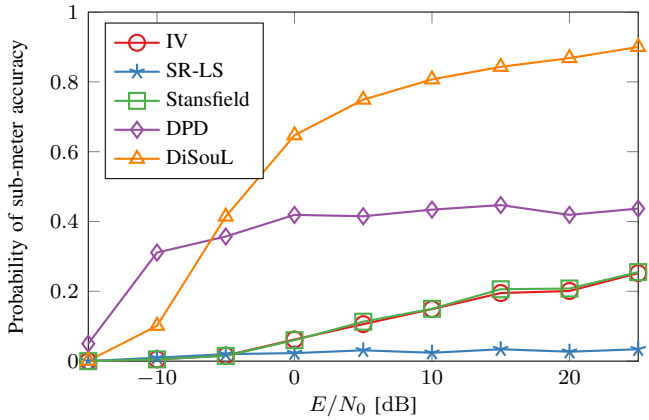Fig. 4. Cumulative density function of the localization error for $E/N_0 = 10\,\mathrm{dB}$ and $B = 30\,\mathrm{MHz}$.

Fig. 6. Probability of sub-meter precision vs. bandwidth for $E/N_0 = 10\,\mathrm{dB}$.

Fig. 5. Probability of sub-meter precision vs. E/N_0 for $B = 30\,\mathrm{MHz}$.

Fig. 7. Probability of sub-meter precision vs. number of antennas at each base station for $E/N_0 = 10\,\mathrm{dB}$ and $B = 30\,\mathrm{MHz}$. The diameter of all BSs UCAs grows linearly with the number of antennas according to the formula $0.5\pi^{-1}\lambda S_l$. For 10 antennas the diameter is $7\,\mathrm{cm}$ and for 120 antennas is $82\,\mathrm{cm}$.

other techniques for most E/N_0 values. The TOA-based SR-LS performs poorly due to the positive bias of the TOA estimates. The AOA-based estimators can slightly improve on this performance, but are still worse than both direct localization approaches. As E/N_0 increases, we sample the snapshots at the time of crossing a threshold rather than at the peak (see Section III-B), which reduces the amount of NLOS multipath components that are included into the snapshots, but the resulting ratio between LOS energy and noise is more or less independent of E/N_0. Thus, the benefit of increased E/N_0 is that we detect the signals sooner, thus diminishing the number of NLOS components making into the snapshots. In the low SNR regime (less than $-5\,\mathrm{dB}$ in the figure), DiSouL is outperformed by DPD because the threshold matched filter used for sampling the signals and estimating the TOA may fail to detect any signal.

Fig. 6 plots the probability of sub-meter accuracy versus signal bandwidth. All techniques benefit from an increase of bandwidth. On the one hand, it is well known that a larger bandwidth results in better TOA estimates. On the other hand, since the pulse width is inversely proportional to the bandwidth, a larger bandwidth results in a shorter pulse. Hence, fewer NLOS multipath components are included into the snapshots (8), thus, decreasing the risk of errors in the

AOA estimation.

Fig. 7 evaluates the probability of sub-meter accuracy versus the number of antennas in each base station. To keep the separation between two neighboring antennas in each UCA equal to $\frac{\lambda}{2}$, the diameter of the array in BS l is increased with the number of antennas according to the formula $\frac{\lambda}{2\sin(\pi/S_l)}$. For ten or more antennas, the expression of the diameter is well approximated by $\frac{\lambda S_l}{2\pi}$, meaning that the array size grows proportionally to the number of antennas S_l, which is directly related to the angular resolution. This improvement in angular resolution allows DiSouL to resolve more multipath arrivals more precisely, and consequently, improve its localization accuracy as observed in Fig. 7. Between 10 and 80 antennas, DiSouL's probability of sub-meter accuracy improves linearly with the number of antennas, and then it saturates. A perfect probability of 1 is not achieved because the assumptions made by DiSouL (see Section IV-B) may not always hold true in the simulated multipath channel. On the contrary, the probability of sub-meter accuracy for the indirect techniques remains approximately the same. In particular, because SR-LS is purely TOA-based, the improvement in angular resolution has no impact. The other two indirect techniques, IV and Stansfield,
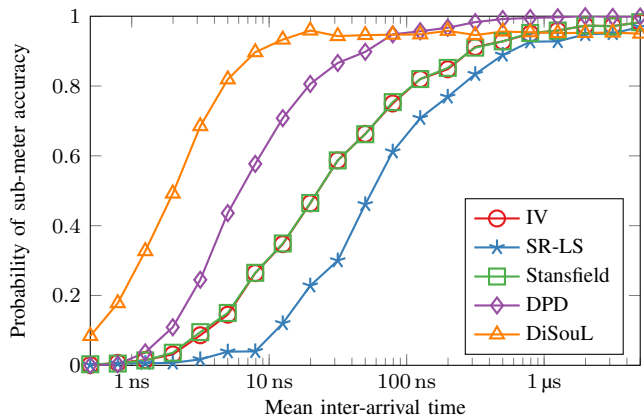
Fig. 8. Probability of sub-meter precision vs. ray mean arrival time for $E/N_0 = 10\,\mathrm{dB}$ and $B = 30\,\mathrm{MHz}$.
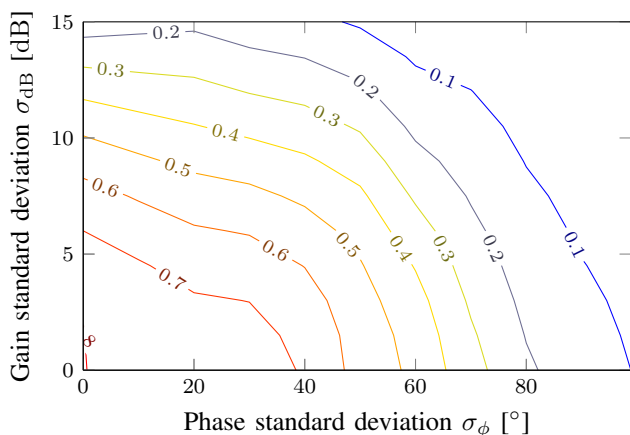
Fig. 9. Contour plot of DiSouL's probability of sub-meter precision vs. gain and phase mismatches on the antennas of all BSs. SNR and bandwidth set to $E/N_0 = 10\,\mathrm{dB}$ and $B = 30\,\mathrm{MHz}$, respectively.

TABLE I
AVERAGE EXECUTION TIMES OF THE MULTIPLE LOCALIZATION TECHNIQUES.

	IV	SR-LS	Stansfield	DPD	DiSouL
Average execution time	0.26 ms	4.3 ms	0.13 ms	33 ms	1.7 s

where $\mathbf{a}_l$ is the nominal (i.e., the array response used by DiSouL) array response (6), and $g_{l,a} \geq 0$ and $\phi_{l,a}$ represent the unknown gains and phases, respectively, of the antennas. The gains (in dB) and phases of all antennas are drawn independently from Gaussian distributions, i.e. $20\log_{10} g_{l,a} \sim \mathcal{N}(\bar{g}_{\mathrm{dB}}, \sigma_{\mathrm{dB}}^2)$ and $\phi_{l,a} \sim \mathcal{N}(0, \sigma_\phi^2)$, where $\bar{g}_{\mathrm{dB}} = -\frac{\ln(10)}{40}\sigma_{\mathrm{dB}}^2$ because it makes $\mathbb{E}\, g_{l,a} = 1$. When the nominal array response matches the true one (i.e., $\sigma_{\mathrm{dB}} = \sigma_\phi = 0$), the probability of sub-meter accuracy is approximately 0.8. Obviously, as larger gain and phase errors occur at all antennas, the performance of DiSouL degrades. The probability of sub-meter accuracy drops from 0.8 to 0.7 at $38°$ phase standard deviation (in the absence of gain mismatches), or at $6\,\mathrm{dB}$ gain standard deviation (in the absence of phase mismatches). Thus, DiSouL is remarkably robust to calibration errors.

Lastly, Table I plots the execution times of all techniques in a regular 3.6 GHz desktop computer. All stations are equipped with 70-antenna arrays. Due to the joint processing of the data at all base stations, the execution times of the direct techniques are much larger than those of the indirect techniques. In particular, DiSouL is substantially more computationally intensive than the other techniques because it needs to solve a relatively large optimization problem multiple times. Instead of using an off-the-shelf solver [43], it may be worth developing/using an algorithm that exploits the sparsity of the signals.

improve very little because most of their errors are due to selection of the wrong path as LOS.

In Fig. 8, we tune some of the channel parameters controlling the rate of arrivals. In the statistical multipath channel model of [15], the times of arrival of the NLOS components are modeled by two parameters: the cluster arrival rate Λ and the ray arrival rate λ. The measured values for the Clyde building of these two parameters were $1/\Lambda = 17\,\mathrm{ns}$ and $1/\Lambda = 5\,\mathrm{ns}$. In order to study the localization accuracy as a function of the ray arrival time, in Fig. 8, $1/\Lambda$ is varied between $5\,\mathrm{ps}$ and $5\,\mathrm{\mu s}$ while $\Lambda = \frac{5}{17}\lambda$. As the ray inter-arrival time increases, the multipath channel becomes less dense. For very high inter-arrival times, the channel can be considered almost pure LOS, and as expected all techniques improve their localization accuracy.

In Fig. 9, we study the effect of calibration errors on the arrays, more specifically, the degradation in localization accuracy due to mismatches between the true and nominal gains/phases of the antennas. Based on the model in [47], the true array response $\tilde{\mathbf{a}}_l$ is given by

$$\left[\tilde{\mathbf{a}}_l(\theta)\right]_a = g_{l,a} e^{i\phi_{l,a}} \left[\mathbf{a}_l(\theta)\right]_a, \tag{29}$$

VII. CONCLUSIONS

This paper tackled the problem of narrowband localization in the presence of multipath, through a direct localization approach in a massive MIMO setting. We propose an original compressive sensing approach for the localization of sources emitting known narrow-band signals. Due to the high angular resolution of massive arrays, it is possible to estimate the AOAs of the multipath components. By jointly processing snapshots of several widely distributed arrays, we are able to estimate the source location precisely without explicitly estimating the LOS AOAs, and therefore, avoiding the challenging data association problem. The proposed technique, called DiSouL, achieves sub-meter localization with high probability in dense multipath environments with narrow-band signals. DiSouL requires no statistical channel knowledge except for the noise variance and therefore it is suitable for any multipath environment. Coarse TOA estimates at each array are used to reduce the execution time and enhance the localization accuracy. Numerical simulations have revealed that DiSouL is also remarkably robust to calibration errors. The large gain in accuracy comes with higher computational complexity compared to previous existing techniques.

APPENDIX A
PROOF OF LEMMA 1

We aim to prove that under A2) and A3), if $w > \sqrt{L-1}$, then any estimated location is consistent with L paths (in the sense of Definition 1). Here the point is that it is more costly (in terms of the objective function) to explain an observation as L NLOS angles, than as one position with L associated LOS angles, and this is so exactly when $w > \sqrt{L-1}$.

Let $\mathbf{X}$ and $\{\mathbf{y}\}_{l=1}^{L}$ be a solution from (17) with cost C_1, and let $\boldsymbol{\pi}_1$ be an estimated location (i.e. $\sqrt{\sum_{l=1}^{L}|x_{1l}|^2} \neq 0$). Then $\hat{\mathbf{z}}_l$ can be expressed as

$$\hat{\mathbf{z}}_l = x_{1l}\mathbf{a}_l\left(\theta_l(\boldsymbol{\pi}_1)\right) + y_{1l}\mathbf{a}_l\left(\vartheta_{1l}\right) + \mathbf{e}_l, \quad l = 1, \ldots, L, \quad (30)$$

where $\vartheta_{1l} = \theta_l(\boldsymbol{\pi}_1)$ and $\mathbf{e}_l$ is placeholder of all the terms in the reconstruction $\hat{\mathbf{z}}_l$ that are not related to the location $\boldsymbol{\pi}_1$ or angle ϑ_{1l}

$$\mathbf{e}_l = \sum_{q>1} x_{ql}\mathbf{a}_l\left(\theta_l(\boldsymbol{\pi}_q)\right) + \sum_{m>1} y_{ml}\mathbf{a}_l\left(\vartheta_{ml}\right) \quad l = 1, \ldots, L. \quad (31)$$

Now, if $\|\mathbf{x}_1\|_0 = L$, then $\boldsymbol{\pi}_1$ is consistent with L paths in the sense of Definition 1 due to Assumption A3). Here, $\mathbf{x}_1 = [x_{11} \cdots x_{1L}]^{\mathrm{T}}$ and $\|\cdot\|_0$ is the ℓ_0-norm which counts the number of estimated elements. Hence, we must prove that $w > \sqrt{L-1}$ implies $\|\mathbf{x}_1\|_0 = L$. The proof is by contradiction.

Assume that

$$\|\mathbf{x}_1\|_0 < L. \quad (32)$$

This means that the position is consistent with less than L paths. Now we have another competing reconstruction $\mathbf{X}'$, $\{\mathbf{y}'\}_{l=1}^{L}$ and

$$\hat{\mathbf{z}}_l = \underbrace{(x_{1l} + y_{1l})}_{\doteq y'_{1l}}\mathbf{a}_l\left(\vartheta_{1l}\right) + \mathbf{e}_l \quad \text{for } l = 1, \ldots, L, \quad (33)$$

with $\mathbf{x}'_1 = 0$ and cost C_2. Since $\mathbf{X}$ and $\{\mathbf{y}\}_{l=1}^{L}$ are optimal, $C_1 \leq C_2$. Consider now the two assignments (30) and (33). Ignoring any common coefficients, the cost of (30) is

$$C_1 = w\sqrt{\sum_{l=1}^{L}|x_{1l}|^2} + \sum_{l=1}^{L}|y_{1l}| \quad (34)$$

whereas the cost of (33) is

$$C_2 = \sum_{l=1}^{L}|y'_{1l}| = \sum_{l=1}^{L}|x_{1l} + y_{1l}| \leq \sum_{l=1}^{L}|x_{1l}| + \sum_{l=1}^{L}|y_{1l}|. \quad (35)$$

Since $C_1 \leq C_2$,

$$w\sqrt{\sum_{l=1}^{L}|x_{1l}|^2} \leq \sum_{l=1}^{L}|x_{1l}|. \quad (36)$$

Define the vector function $\mathbb{1}_{\mathbf{x}}$ whose l-th entry is 1 if $x_{1l} \neq 0$, and 0 otherwise, and denote by $\tilde{\mathbf{x}}$ the element-wise absolute value of $\mathbf{x}_1$, i.e. $\tilde{x}_l = |x_{1l}|$. Then, $\|\mathbf{x}_1\|_1 = \mathbb{1}_{\mathbf{x}}^{\mathrm{T}}\tilde{\mathbf{x}}$, so from the Cauchy-Schwarz inequality, it follows immediately that

$$\|\mathbf{x}_1\|_1 \leq \sqrt{\|\mathbf{x}_1\|_0}\|\mathbf{x}_1\|_2. \quad (37)$$

Putting everything together, we find the following contradiction

$$w\|\mathbf{x}_1\|_2 \overset{(36)}{\leq} \|\mathbf{x}_1\|_1 \overset{(37)}{\leq} \sqrt{\|\mathbf{x}_1\|_0}\|\mathbf{x}_1\|_2 \\ \overset{(32)}{\leq} \sqrt{L-1}\|\mathbf{x}_1\|_2 \overset{(a)}{<} w\|\mathbf{x}_1\|_2, \quad (38)$$

where (a) is due to the fact that $w > \sqrt{L-1}$. Hence, $w > \sqrt{L-1}$ implies $\|\mathbf{x}_1\|_0 = L$.

APPENDIX B
PROOF OF LEMMA 2

If no location were found, for each possible location just enough "mass" from each NLOS detected observation could be moved, in a certain way, over to LOS; the new cost cannot exceed the nominal cost if $w < \sqrt{L}$.

The proof is by contradiction. Assume that $w < \sqrt{L}$ and that there is no estimated location output by problem (17), so that $x_{ql} = 0$, $\forall q, l$. Then,

$$\hat{\mathbf{z}}_l = \sum_m y_{ml}\mathbf{a}_l\left(\vartheta_{ml}\right) \quad l = 1, \ldots, L. \quad (39)$$

Assume without loss of generality that $\vartheta_{1l} = \theta_l(\mathbf{p})$. By Assumption A3), $\theta_l(\mathbf{p}) \in \hat{\Theta}_l$, so that $y_{1l} \neq 0$, which leads to the following decomposition

$$\hat{\mathbf{z}}_l = y_{1l}\mathbf{a}_l\left(\vartheta_{1l}\right) + \sum_{m>1} y_{ml}\mathbf{a}_l\left(\vartheta\right) \quad l = 1, \ldots, L. \quad (40)$$

We consider a competing decomposition $\mathbf{X}'$, $\{\mathbf{y}'\}_{l=1}^{L}$, for which $x'_{ql} \neq 0$ for some q, l. In particular, $\boldsymbol{\pi}_1 = \mathbf{p}$; then

$$\hat{\mathbf{z}}_l = x'_{1l}\mathbf{a}_l\left(\theta_l(\boldsymbol{\pi}_1)\right) + \underbrace{(y_{1l} - x'_{1l})}_{\doteq y'_{1l}}\mathbf{a}_l\left(\vartheta_{1l}\right) + \\ + \sum_{m>1} y'_{ml}\mathbf{a}_l\left(\vartheta_{ml}\right) \quad l = 1, \ldots, L, \quad (41)$$

where $y'_{ml} = y_{ml}$ for all l and $m > 1$. Ignoring common terms, we can associate a cost C_1 and C_2 with (40) and (41), respectively, where

$$C_1 = \sum_{l=1}^{L}|y_{1l}| \quad (42)$$

$$C_2 = w\sqrt{\sum_{l=1}^{L}|x'_{1l}|^2} + \sum_{l=1}^{L}|y_{1l} - x'_{1l}|. \quad (43)$$

If we select x'_{1l} such that $|x'_{1l}| = \min_l |y_{1l}|$ and $\angle x'_{1l} = \angle y_{1l}$, and utilize the fact that $C_1 \leq C_2$, we have

$$\sum_{l=1}^{L}|y_{1l}| \leq w\sqrt{L}\min_l |y_{1l}| + \sum_{l=1}^{L}|y_{1l}| - L\min_l |y_{1l}|, \quad (44)$$

implying that $w\sqrt{L} - L \geq 0$, which contradicts $w < \sqrt{L}$.

REFERENCES

[1] T. S. Rappaport, S. Sun, R. Mayzus, H. Zhao, Y. Azar, K. Wang, G. N. Wong, J. K. Schulz, M. Samimi, and F. Gutierrez, "Millimeter wave mobile communications for 5G cellular: It will work!" *IEEE Access*, vol. 1, pp. 335–349, May 2013.

[2] E. G. Larsson, O. Edfors, F. Tufvesson, and T. Marzetta, "Massive MIMO for next generation wireless systems," *IEEE Communications Magazine*, vol. 52, no. 2, pp. 186–195, 2014.

[3] W. H. Chin, Z. Fan, and R. Haines, "Emerging technologies and research challenges for 5G wireless networks," *IEEE Wireless Communications*, vol. 21, no. 2, pp. 106–112, 2014.

[4] A. Guerra, F. Guidi, and D. Dardari, "Position and orientation error bound for wideband massive antenna arrays," in *IEEE International Conference on Communication Workshop*, 2015, pp. 853–858.

[5] V. Savic and E. G. Larsson, "Fingerprinting-based positioning in distributed massive MIMO systems," in *IEEE 82nd Vehicular Technology Conference*, 2015, pp. 1–5.

[6] F. Guidi, A. Guerra, and D. Dardari, "Personal mobile radars with millimeter-wave massive arrays for indoor mapping," *IEEE Transactions on Mobile Computing*, vol. 15, no. 6, pp. 1536–1233, 2016.

[7] ——, "Millimeter-wave massive arrays for indoor SLAM," in *IEEE International Conference on Communications Workshops*, 2014, pp. 114–120.

[8] M. Gavish and A. J. Weiss, "Performance analysis of bearing-only target location algorithms," *IEEE Transactions on Aerospace and Electronic Systems*, vol. 28, no. 3, pp. 817–828, 1992.

[9] L. M. Kaplan, Q. Le, and P. Molnár, "Maximum likelihood methods for bearings-only target localization," in *IEEE International Conference on Acoustics, Speech, and Signal Processing*, vol. 5, 2001, pp. 3001–3004.

[10] K. Doğançay, "Passive emitter localization using weighted instrumental variables," *Signal processing*, vol. 84, no. 3, pp. 487–497, 2003.

[11] S. Azzouzi, M. Cremer, U. Dettmar, R. Kronberger, and T. Knie, "New measurement results for the localization of UHF RFID transponders using an angle of arrival (AOA) approach," in *IEEE International Conference on RFID*, 2011, pp. 91–97.

[12] A. Hu, T. Lv, H. Gao, Z. Zhang, and S. Yang, "An ESPRIT-based approach for 2-D localization of incoherently distributed sources in massive MIMO systems," *IEEE Journal of Selected Topics in Signal Processing*, vol. 8, no. 5, pp. 996–1011, 2014.

[13] T. Lv, F. Tan, H. Gao, and S. Yang, "A beamspace approach for 2-D localization of incoherently distributed sources in massive MIMO systems," *Signal Processing*, vol. 121, pp. 30–45, 2016.

[14] R. Klukas and M. Fattouche, "Line-of-sight angle of arrival estimation in the outdoor multipath environment," *IEEE Transactions on Vehicular Technology*, vol. 47, no. 1, pp. 342–351, 1998.

[15] Q. H. Spencer, B. D. Jeffs, M. Jensen *et al.*, "Modeling the statistical time and angle of arrival characteristics of an indoor multipath channel," *IEEE Journal on Selected Areas in Communications*, vol. 18, no. 3, pp. 347–360, 2000.

[16] S. Sen, J. Lee, K.-H. Kim, and P. Congdon, "Avoiding multipath to revive inbuilding wifi localization," in *11th Annual International Conference on Mobile Systems, Applications, and Services*. ACM, 2013, pp. 249–262.

[17] K. R. Pattipati, S. Deb, Y. Bar-Shalom, and R. B. Washburn Jr, "A new relaxation algorithm and passive sensor data association," *IEEE Transactions on Automatic Control*, vol. 37, no. 2, pp. 198–213, 1992.

[18] A. J. Weiss, "Direct position determination of narrowband radio frequency transmitters," *IEEE Signal Processing Letters*, vol. 11, no. 5, pp. 513–516, 2004.

[19] M. Wax, T.-J. Shan, and T. Kailath, "Location and the spectral density estimation of multiple sources," DTIC Document, Tech. Rep., 1982.

[20] M. Wax and T. Kailath, "Optimum localization of multiple sources by passive arrays," *IEEE Transactions on Acoustics, Speech and Signal Processing*, vol. 31, no. 5, pp. 1210–1217, 1983.

[21] ——, "Decentralized processing in sensor arrays," *IEEE Transactions on Acoustics, Speech and Signal Processing*, vol. 33, no. 5, pp. 1123–1129, 1985.

[22] A. J. Weiss and A. Amar, "Direct position determination of multiple radio signals," *EURASIP Journal on Applied Signal Processing*, vol. 2005, no. 1, pp. 37–49, 2005.

[23] J. C. Chen, R. E. Hudson, and K. Yao, "Maximum-likelihood source localization and unknown sensor location estimation for wideband signals in the near-field," *IEEE Transactions on Signal Processing*, vol. 50, no. 8, pp. 1843–1854, 2002.

[24] O. Bialer, D. Raphaeli, and A. J. Weiss, "Maximum-likelihood direct position estimation in dense multipath," *IEEE Transactions on Vehicular Technology*, vol. 62, no. 5, pp. 2069–2079, 2013.

[25] "C-RAN: the road towards green RAN," White Paper, China Mobile, October 2011.

[26] J. Wu, S. Rangan, and H. Zhang, *Green communications: theoretical fundamentals, algorithms and applications*. CRC Press, 2012.

[27] N. Garcia, A. M. Haimovich, J. A. Dabin, M. Coulon, and M. Lops, "Direct localization of emitters using widely spaced sensors in multipath environments," in *48th Asilomar Conference on Signals, Systems and Computers*. IEEE, 2014, pp. 695–700.

[28] D. Dardari, C.-C. Chong, and M. Z. Win, "Threshold-based time-of-arrival estimators in UWB dense multipath channels," *IEEE Transactions on Communications*, vol. 56, no. 8, pp. 1366–1378, 2008.

[29] D. Malioutov, M. Çetin, and A. S. Willsky, "A sparse signal reconstruction perspective for source localization with sensor arrays," *IEEE Transactions on Signal Processing*, vol. 53, no. 8, pp. 3010–3022, 2005.

[30] F. Rusek, D. Persson, B. K. Lau, E. G. Larsson, T. L. Marzetta, O. Edfors, and F. Tufvesson, "Scaling up MIMO: Opportunities and challenges with very large arrays," *IEEE Signal Processing Magazine*, vol. 30, no. 1, pp. 40–60, 2013.

[31] J. Vieira, S. Malkowsky, K. Nieman, Z. Miers, N. Kundargi, L. Liu, I. Wong, V. Öwall, O. Edfors, and F. Tufvesson, "A flexible 100-antenna testbed for massive MIMO," in *2014 IEEE Globecom Workshops*, 2014, pp. 287–293.

[32] I. Cespedes, Y. Huang, J. Ophir, and S. Spratt, "Methods for estimation of subsample time delays of digitized echo signals," *Ultrasonic imaging*, vol. 17, no. 2, pp. 142–171, 1995.

[33] J. A. Tropp, "Algorithms for simultaneous sparse approximation. Part II: Convex relaxation," *Signal Processing*, vol. 86, no. 3, pp. 589–602, 2006.

[34] S. T. Smith, "Statistical resolution limits and the complexified Cramér-Rao bound," *IEEE Transactions on Signal Processing*, vol. 53, no. 5, pp. 1597–1609, 2005.

[35] E. J. Candès and C. Fernandez-Granda, "Towards a mathematical theory of super-resolution," *Communications on Pure and Applied Mathematics*, vol. 67, no. 6, pp. 906–956, 2014.

[36] J.-J. Fuchs, "Multipath time-delay detection and estimation," *IEEE Transactions on Signal Processing*, vol. 47, no. 1, pp. 237–243, 1999.

[37] L. Jacob, G. Obozinski, and J.-P. Vert, "Group lasso with overlap and graph lasso," in *26th Annual International Conference on Machine Learning*. ACM, 2009, pp. 433–440.

[38] M. S. Lobo, L. Vandenberghe, S. Boyd, and H. Lebret, "Applications of second-order cone programming," *Linear algebra and its applications*, vol. 284, no. 1, pp. 193–228, 1998.

[39] M. M. Hyder and K. Mahata, "Direction-of-arrival estimation using a mixed norm approximation," *IEEE Transactions on Signal Processing*, vol. 58, no. 9, pp. 4646–4655, 2010.

[40] E. Schechter, *Handbook of Analysis and its Foundations*. Academic Press, 1996.

[41] J.-J. Fuchs, "On the application of the global matched filter to DOA estimation with uniform circular arrays," *IEEE Transactions on Signal Processing*, vol. 49, no. 4, pp. 702–709, 2001.

[42] *Standard Test Procedures for Antennas*, IEEE Std. 149–1979, 1979.

[43] MOSEK ApS, "The MOSEK optimization toolbox for MATLAB manual, version 7.1 (revision 51)," http://mosek.com, (accessed on March 20, 2016).

[44] A. Beck, P. Stoica, and J. Li, "Exact and approximate solutions of source localization problems," *IEEE Transactions on Signal Processing*, vol. 56, no. 5, pp. 1770–1778, 2008.

[45] L. C. Godara, "Application of antenna arrays to mobile communications. II. Beam-forming and direction-of-arrival considerations," *Proceedings of the IEEE*, vol. 85, no. 8, pp. 1195–1245, 1997.

[46] R. O. Schmidt, "Multiple emitter location and signal parameter estimation," *IEEE Transactions on Antennas and Propagation*, vol. 34, no. 3, pp. 276–280, 1986.

[47] B. Friedlander, "A sensitivity analysis of the MUSIC algorithm," *IEEE Transactions on acoustics, speech, and signal processing*, vol. 38, no. 10, pp. 1740–1751, 1990.

Nil Garcia (S'14–M'16) received the Telecommunications Engineer degree from the Polytechnic University of Catalonia (UPC), Barcelona, Spain, in 2008; and the double Ph.D. degree in electrical engineering from the New Jersey Institute of Technology, Newark, NJ, USA, and from the National Polytechnic Institute of Toulouse, Toulouse, France, in 2015.

He is currently a postdoctoral researcher of Communication Systems with the Department of Signals and Systems at Chalmers University of Technology, Sweden. In 2009, he worked was an engineer in the Centre National d'Études Spatiales (CNES). In 2008 and 2009, he had internships in CNES and NASA. Hi research interests are in the areas of localization, intelligent transportation systems and 5G.

Erik G. Larsson received the Ph.D. degree from Uppsala University, Uppsala, Sweden, in 2002.

He is currently Professor of Communication Systems at Linköping University (LiU) in Linköping, Sweden. He was with the Royal Institute of Technology (KTH) in Stockholm, Sweden, the University of Florida, USA, the George Washington University, USA, and Ericsson Research, Sweden. In 2015 he was a Visiting Fellow at Princeton University, USA, for four months. His main professional interests are within the areas of wireless communications and signal processing. He has co-authored some 130 journal papers on these topics, he is co-author of the two Cambridge University Press textbooks *Space-Time Block Coding for Wireless Communications* (2003) and *Fundamentals of Massive MIMO* (2016). He is co-inventor on 16 issued and many pending patents on wireless technology.

He was Associate Editor for, among others, the *IEEE Transactions on Communications* (2010–2014) and the *IEEE Transactions on Signal Processing* (2006–2010). From 2015 to 2016 he served as chair of the IEEE Signal Processing Society SPCOM technical committee, and in 2017 he is the past chair of this committee. From 2014 to 2015 he served as chair of the steering committee for the *IEEE Wireless Communications Letters*. He was the General Chair of the Asilomar Conference on Signals, Systems and Computers in 2015, its Technical Chair in 2012. He is a member of the IEEE Signal Processing Society Awards Board during 2017–2019.

He received the IEEE Signal Processing Magazine Best Column Award twice, in 2012 and 2014, and the IEEE ComSoc Stephen O. Rice Prize in Communications Theory in 2015.

Alexander M. Haimovich (S'82–M'87–F'13) received the B.Sc. degree in electrical engineering from the Technion?Israel Institute of Technology, Haifa, in 1977, the M.Sc. degree in electrical engineering from Drexel University, Philadelphia, in 1983, and the Ph.D. degree in systems from the University of Pennsylvania, Philadelphia, in 1989.

From 1983 to 1990, he was a design engineer and staff consultant at AEL Industries. He served as Chief Scientist of JJM Systems from 1990 until 1992. Since 1992 he has been on the faculty at the New Jersey Institute of Technology, where he currently serves as the Ying Wu Chair and Distinguished Professor in the Electrical and Computer Engineering department. He also serves as the Director of the Elisha Bar-Ness Center for Wireless Information Processing. His research interests include MIMO radar, active and passive localization, signal intelligence, sensor networks and wireless networks.

Henk Wymeersch (S'01–M'05) obtained the Ph.D. degree in Electrical Engineering/Applied Sciences in 2005 from Ghent University, Belgium.

He is currently a Professor of Communication Systems with the Department of Signals and Systems at Chalmers University of Technology, Sweden. Prior to joining Chalmers, he was a postdoctoral researcher from 2005 until 2009 with the Laboratory for Information and Decision Systems at the Massachusetts Institute of Technology.

Prof. Wymeersch served as Associate Editor for IEEE Communication Letters (2009–2013), IEEE Transactions on Wireless Communications (since 2013), and IEEE Transactions on Communications (since 2016). His current research interests include cooperative systems and intelligent transportation.

Martial Coulon received the Ingénieur degree in computer science and applied mathematics from ENSEEIHT (Toulouse Engineering School), and the M.Sc. degree in signal processing from the National Polytechnic Institute of Toulouse (INPT), France, both in 1996. He received the Ph.D. degree from INPT in 1999.

Since 2013, he has been a Full Professor with the University of Toulouse, (INPT-ENSEEIHT, Department of Communications Systems), and a member of the IRIT laboratory (CNRS). His research activities are centred around statistical signal processing and communications systems, with a particular interest to change-point detection, Bayesian inference, spread spectrum systems, multiuser detection and cognitive radio.